Supplemental Document

PHOTONICS Research

Axial gradient excitation accelerates volumetric imaging of two-photon microscopy

YUFENG GAO[1,2,†], XIANYUAN XIA[1,2,†], LINA LIU[1,2], TING WU[1,2], TINGAI CHEN[1,2], JIA YU[1,2], ZHILI XU[3], LIANG WANG[1,2], FEI YAN[3], ZHUO DU[4,5], JUN CHU[1,2], YANG ZHAN[6], BO PENG[7], HUI LI[1,2], WEI ZHENG[1,2]

[1]Research Center for Biomedical Optics and Molecular Imaging, Shenzhen Key Laboratory for Molecular Imaging, Guangdong Provincial Key Laboratory of Biomedical Optical Imaging Technology, Shenzhen Institute of Advanced Technology, Chinese Academy of Sciences, Shenzhen 518055, China

[2]CAS Key Laboratory of Health Informatics, Shenzhen Institute of Advanced Technology, Chinese Academy of Sciences, Shenzhen 518055, China

[3]Paul C. Lauterbur Research Center for Biomedical Imaging, Institute of Biomedical and Health Engineering, Shenzhen Institute of Advanced Technology, Chinese Academy of Sciences, Shenzhen, 518055, China

[4]State Key Laboratory of Molecular Developmental Biology, Institute of Genetics and Developmental Biology, Chinese Academy of Sciences, Beijing 100101, China

[5]Key Laboratory of Genetic Network Biology, Institute of Genetics and Developmental Biology, Chinese Academy of Sciences, Beijing 100101, China

[6]Brain Cognition and Brain Disease Institute, Shenzhen Institute of Advanced Technology, Chinese Academy of Sciences, Shenzhen 518055, China

[7]Centre for Micro Nano Systems and Bionic Medicine, Shenzhen Institute of Advanced Technology, Chinese Academy of Sciences, Shenzhen 518055, China

† These authors contributed equally to this work

hui.li@siat.ac.cn

zhengwei@siat.ac.cn

Contents

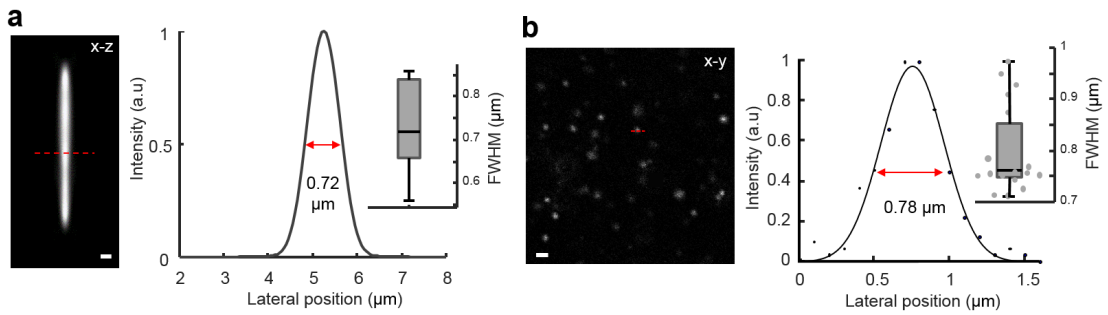

Fig. S1 Theoretical and experimentally measured lateral resolutions. (**a**) Left, square of simulated point spread function of Grad-TPM (PSF^2). Scale bar, 1 μm. Right, lateral profile across middle of PSF^2 (dashed red line on left panel), and statistical result of lateral resolutions calculated from different depths of PSF^2. Squaring is necessary because intensity of two-photon excitation fluorescence is proportional to square of excitation intensity. (**b**) Left, exemplary image of 100-nm-diameter yellow–green fluorescence beads in gel used for measuring actual resolution of Grad-TPM system. Scale bar, 2 μm. Right, profile across middle of representative bead (dashed red line on left panel) with corresponding Gaussian fitting result and statistical result of lateral resolutions calculated from different beads (n = 20).

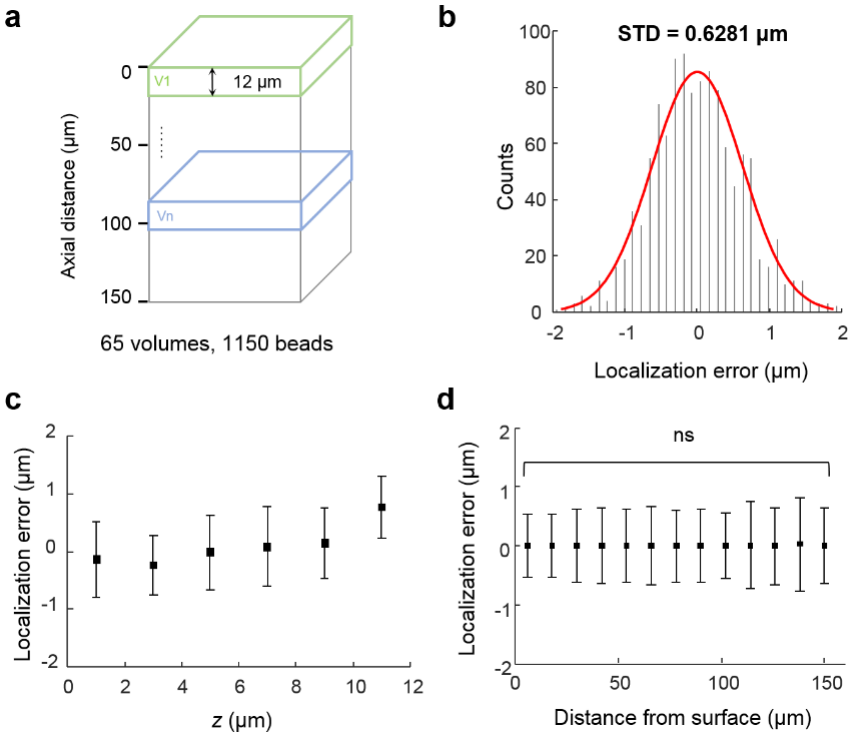

Fig. S2 Axial localization error analysis on experimental data of Fig. 1c. (**a**) Imaging volume of the experimental data. (**b**) Histogram of the localization error. (**c**) Localization error as a function of depth in a single Grad-TPM volume. (**d**) Localization error as a function of the distance from sample surface.

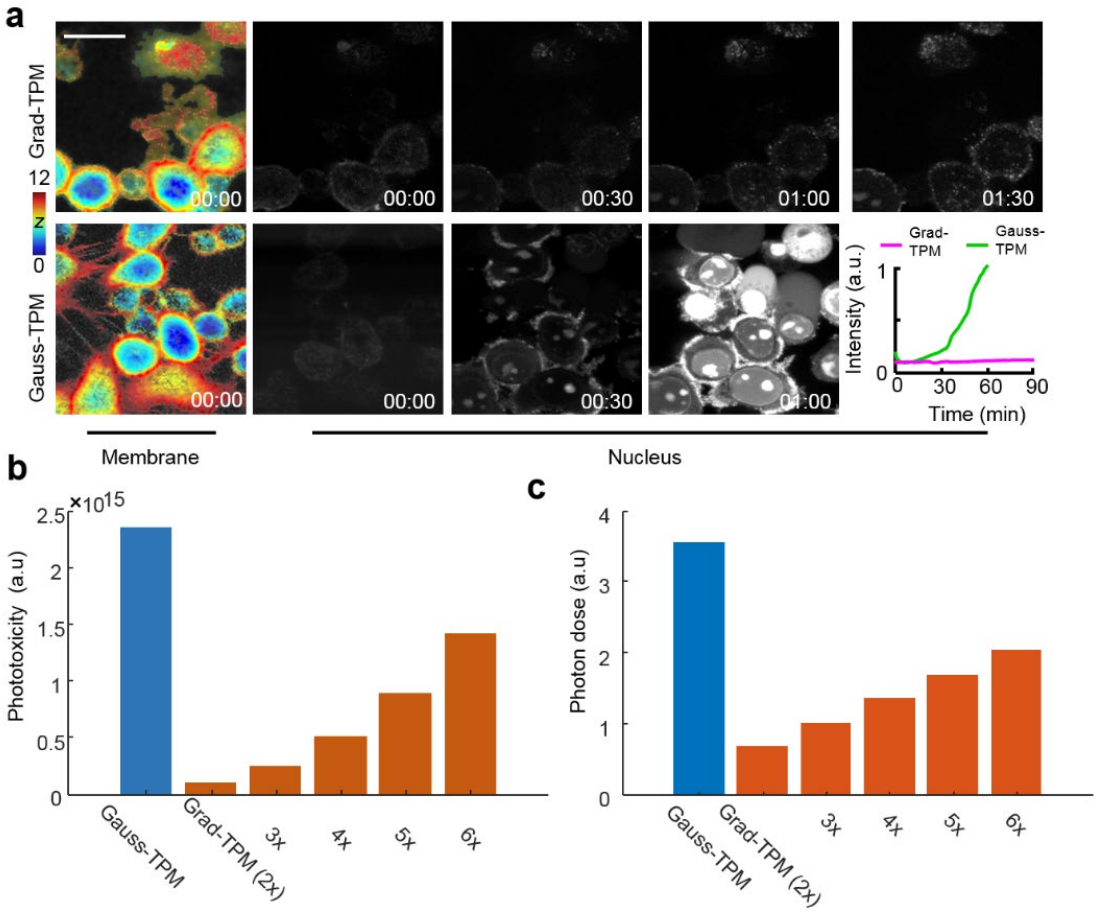

Fig. S3 Phototoxicity assessment. (**a**) Time-lapse imaging on living HepG2 cells via Grad-TPM shows observably lower phototoxicity compared with traditional Gauss-TPM. Cell membrane and nucleus were labeled with DyLight 488 and PI, respectively. PI cannot cross the membrane of live cells and appear bright only if it binds to the nucleic acids after the cell is dead. Lower right graph is created by calculating average intensity of entire nucleus image at each time point. Scale bars, 20 μm. Time is shown at corner as h:min. Units of z: μm. (**b**) Theoretical phototoxicity comparison of Grad-TPM and Gauss-TPM. 2-6× indicate that excitation power of Grad-TPM is two to six times that of the Gauss-TPM. **c,** Theoretical photon-dose comparison. In TPM, phototoxicity and photon dose has been shown to scale as $\int I(\vec{x},t)^{2.5}\,dV\,dt$ and $\int I(\vec{x},t)\,dV\,dt$, respectively, where $I(\vec{x},t)$ is the intensity distribution; V the excited volume, and t the time. Here, we used a cylindrical volume of a radius of 6 μm and a height of 30 μm, and took the focal point as the coordinate center.

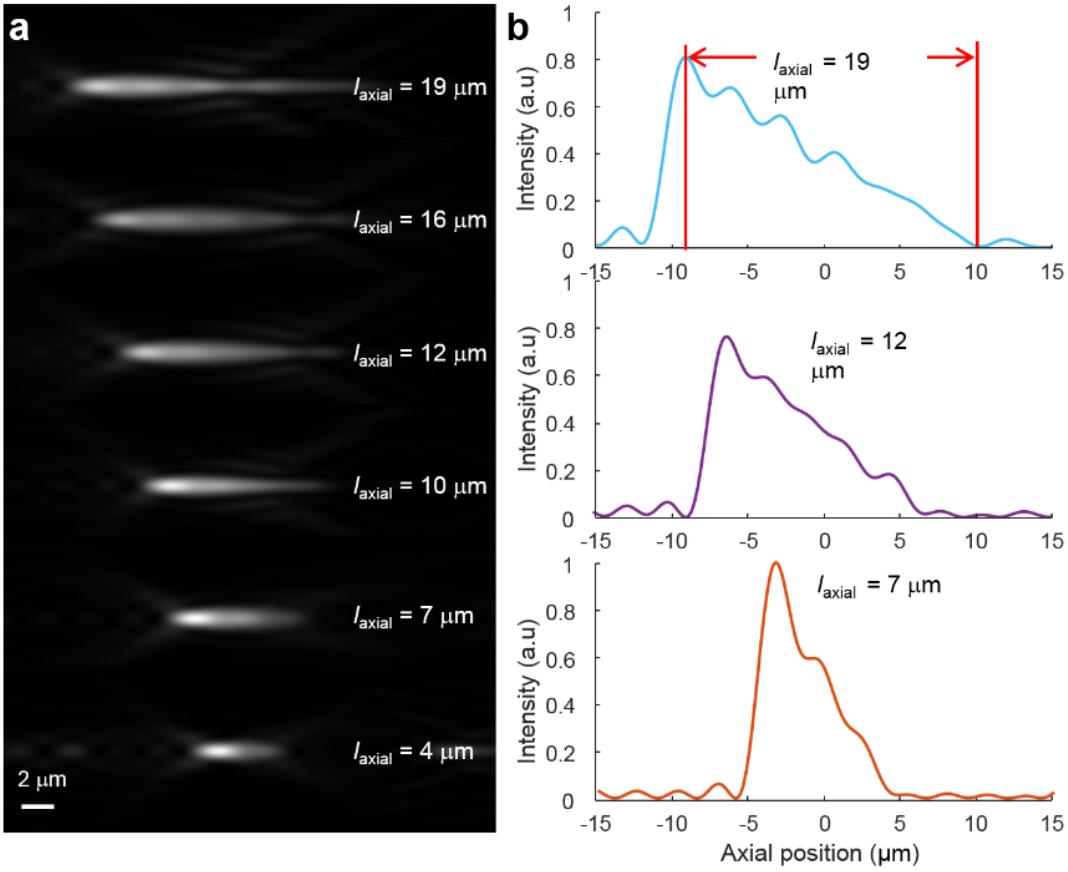

Fig. S4 Gradient foci with different lengths. (**a**) Theoretical intensity distributions calculated using Richards–Wolf theory and varied from 4 to 20 in focal region. Scale bar, 2 μm. (**b**) Corresponding profiles of 7, 12, and 19 μm gradient foci along optical axis. These profile indicate that 12 μm is favorable for Grad-TPM considering smoothness of slope, maximum intensity, and focal length.

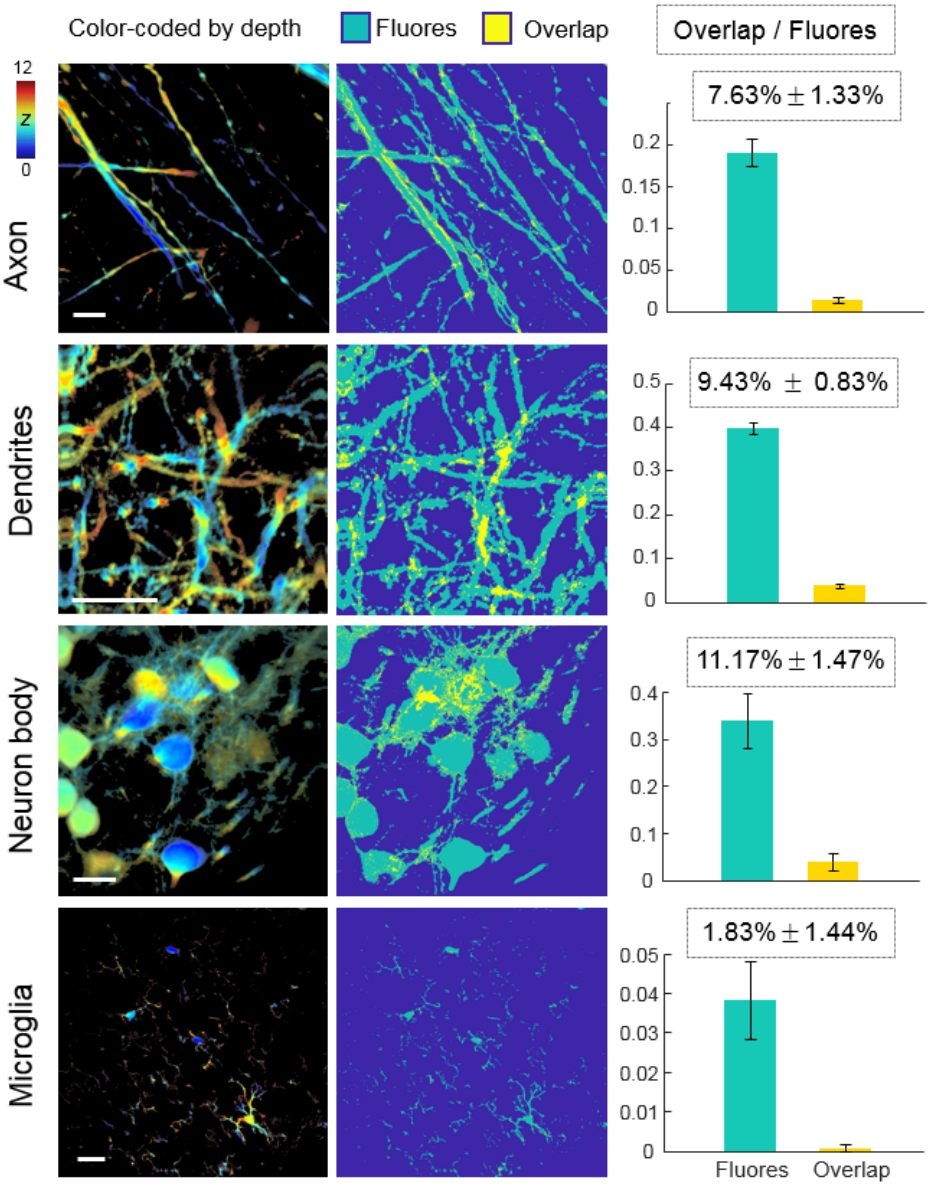

Fig. S5 Evaluation of the axial overlap of different cellular structures in brain slices. Fluores: fluorescent structures; Overlap, where two or more structures overlaps within the 12-μm axial range. The ratio of the overlap area to the total fluorescent area (measured on Gauss-TPM images) ranges from 1.83% to 11.17%, suggesting that many structures are sparsely distributed in the 12-μm axial range. Therefore, the Grad-TPM method is suitable for imaging brains slices. Unit of z: μm.

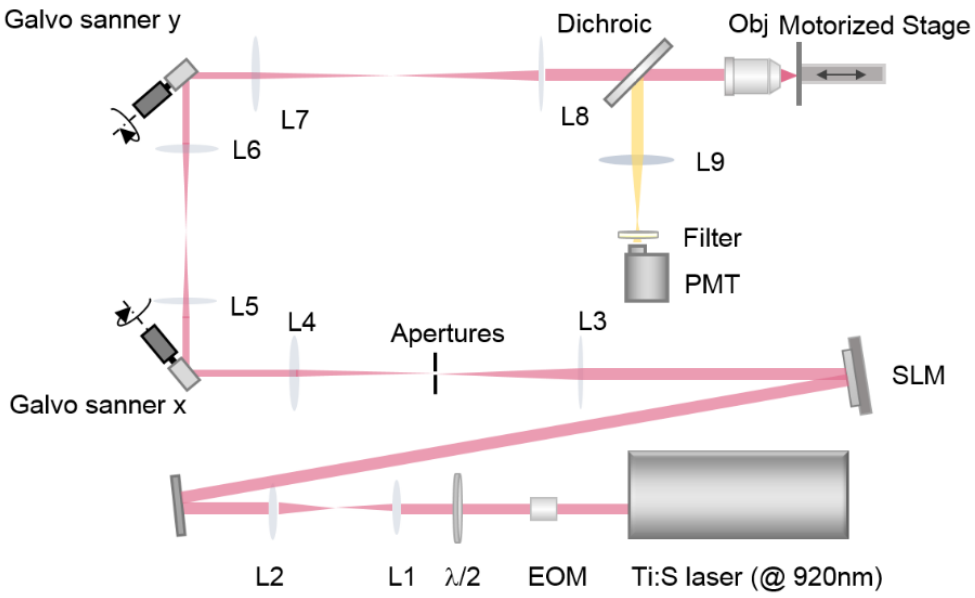

Fig. S6 Gradient two-photon excitation microscope setup. EOM, electro–optical modulator; λ/2, 1/2 λ wave plate; L, lens; SLM, spatial light modulator; Obj, objective lens; PMT, photomultiplier.

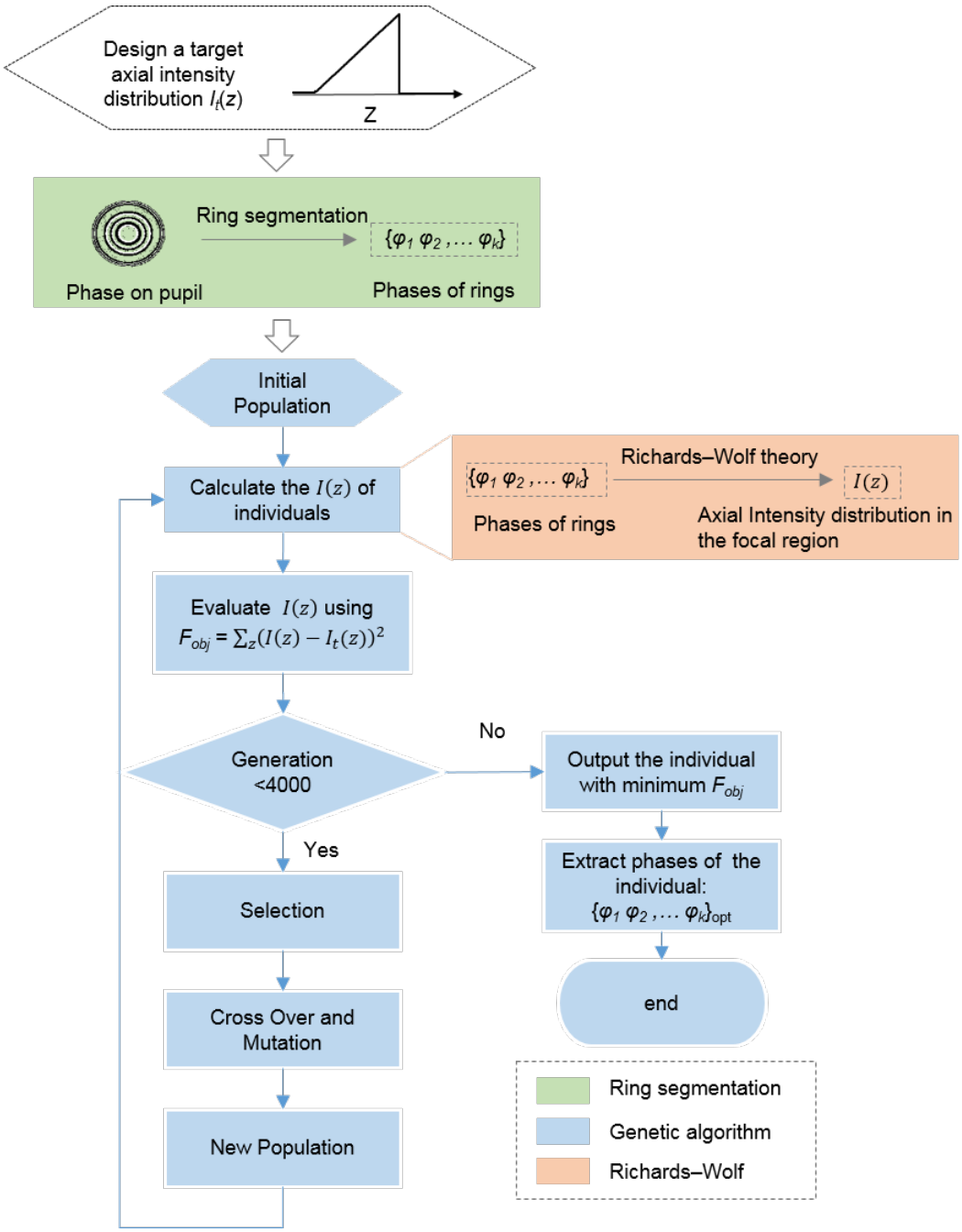

Fig. S7 Gradient focus generation flowchart. $I_t(z)$: the target axial excitation intensity profile; $I(z)$: the axial excitation intensity profile calculated with the pupil phase $\{\varphi_1 \varphi_2, \ldots \varphi_k\}$, and $\{\varphi_1 \varphi_2, \ldots \varphi_k\}$ denote the phase of each ring on the pupil; F_{obj}: the objective function to evaluate the fitness of $I(z)$ and used for individual selection; $\{\varphi_1 \varphi_2, \ldots \varphi_k\}_{opt}$ is the optimal pupil phase generating target gradient focus.

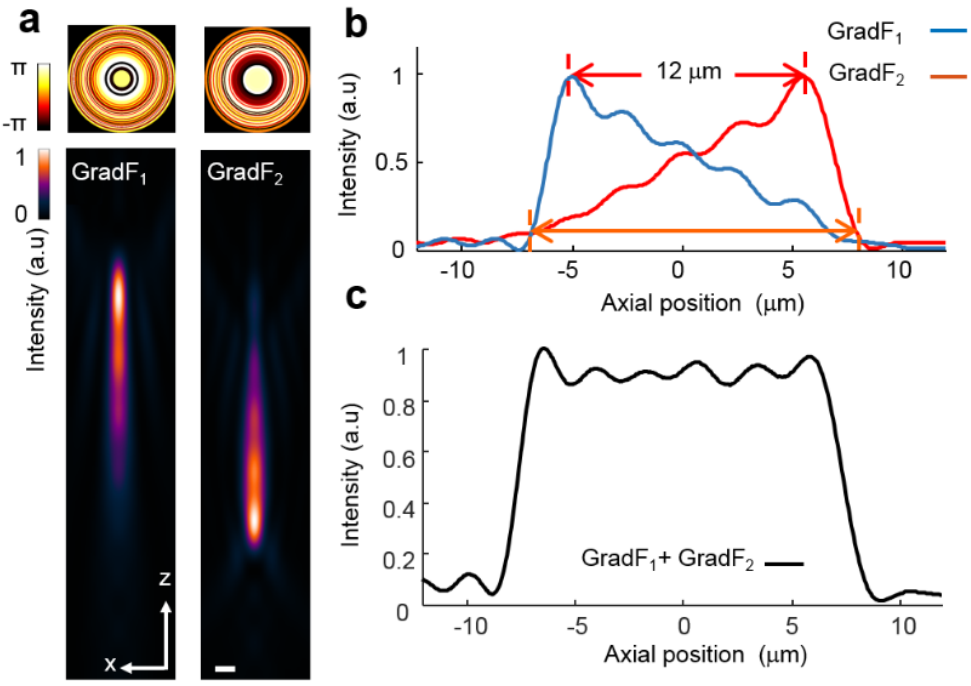

Fig. S8 Simulated gradient excitation focus pair. (**a**) Axial views of PSFs of the gradient excitation focus pair ($GradF_1$ and $GradF_2$) and corresponding phase patterns that generate the PSFs. Scale bar, 1 μm. (**b**) Intensity profiles of the two gradient excitation foci along the optical axis. (**c**) Sum of the axial intensity profiles of gradient excitation focus pair.

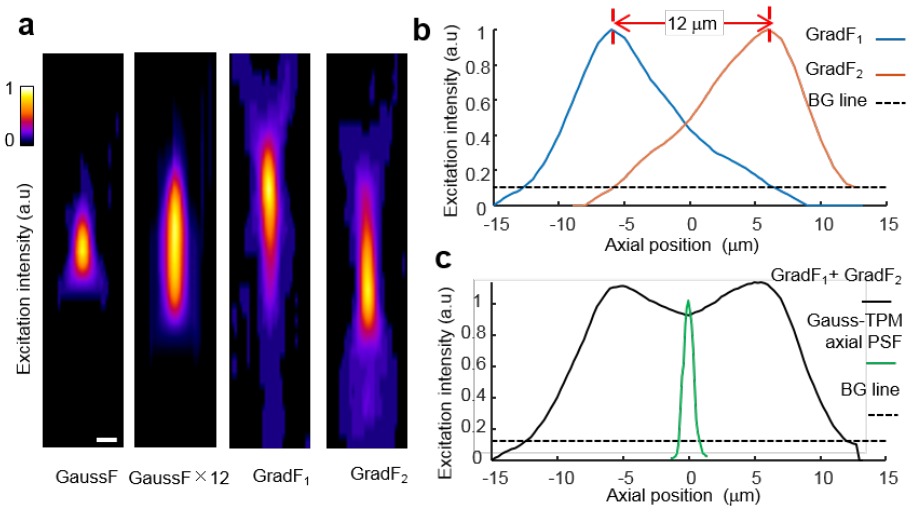

Fig. S9 Experimental gradient focus pair measured using 1-μm-diameter fluorescent beads. (**a**) Axial-view images of 1 μm fluorescent bead indicating PSFs of Gaussian focus (GaussF), axially cascaded Gaussian foci (GaussF × 12), gradient foci 1 and 2 ($GradF_1$ and $GradF_2$, respectively) from left to right. Scale bar, 1 μm. Note that given the nonlinear effect of two-photon excitation, the emission intensity of the beads was translated to excitation intensity for display. (**b**) Measured excitation intensity profiles of GradF1 and GradF2 along optical axis. (**c**) Measured axial excitation intensity profile of sum of $GradF_1$ and $GradF_2$. The profile of Gaussian focus was also presented for comparison. BG: background.

We measured the PSF of the gradient focus by performing a 3D scanning of a 1-μm-diameter bead within a voxel size of 0.25 μm × 0.25 μm × 1 μm. Because the PSF was undersampled in the axial direction, the resulting PSF was interpolated linearly along the optical axis by a factor of four and then filtered by a 3D Gaussian blur with a radius of one voxel. The square root of the obtained images was used to determine the actual distribution of the excitation light around the focus because the intensity of two-photon excitation fluorescence is proportional to the square of the excitation intensity.

As shown in **b,** the gradient focus exhibits an intensity tail (at the maximum-intensity end) outside the designed axial range. Although we attempted to create an extremely steep tail, some outside fluorophores may still be excited, and their axial locations will be incorrectly estimated. To alleviate this effect, we first adjusted the axial displacement between the pair of foci such that the excitation intensity of one focus is sufficiently small outside the designed axial range. Subsequently, a threshold (BG line in **b**) was empirically selected to exclude the outside fluorophores. Hence, the outside fluorophores excited by the tail at the maximum-intensity end of a focus were located outside of the minimum-intensity end of another focus (under the BG line). These fluorophores will yield an outlier intensity ratio when one of the pairs of intensities becomes negligible. Finally, we carefully determined the intensity ratio range corresponding to the designed axial range and ascribed the fluorophore with an outlier intensity ratio to the nearest available position (top or bottom).

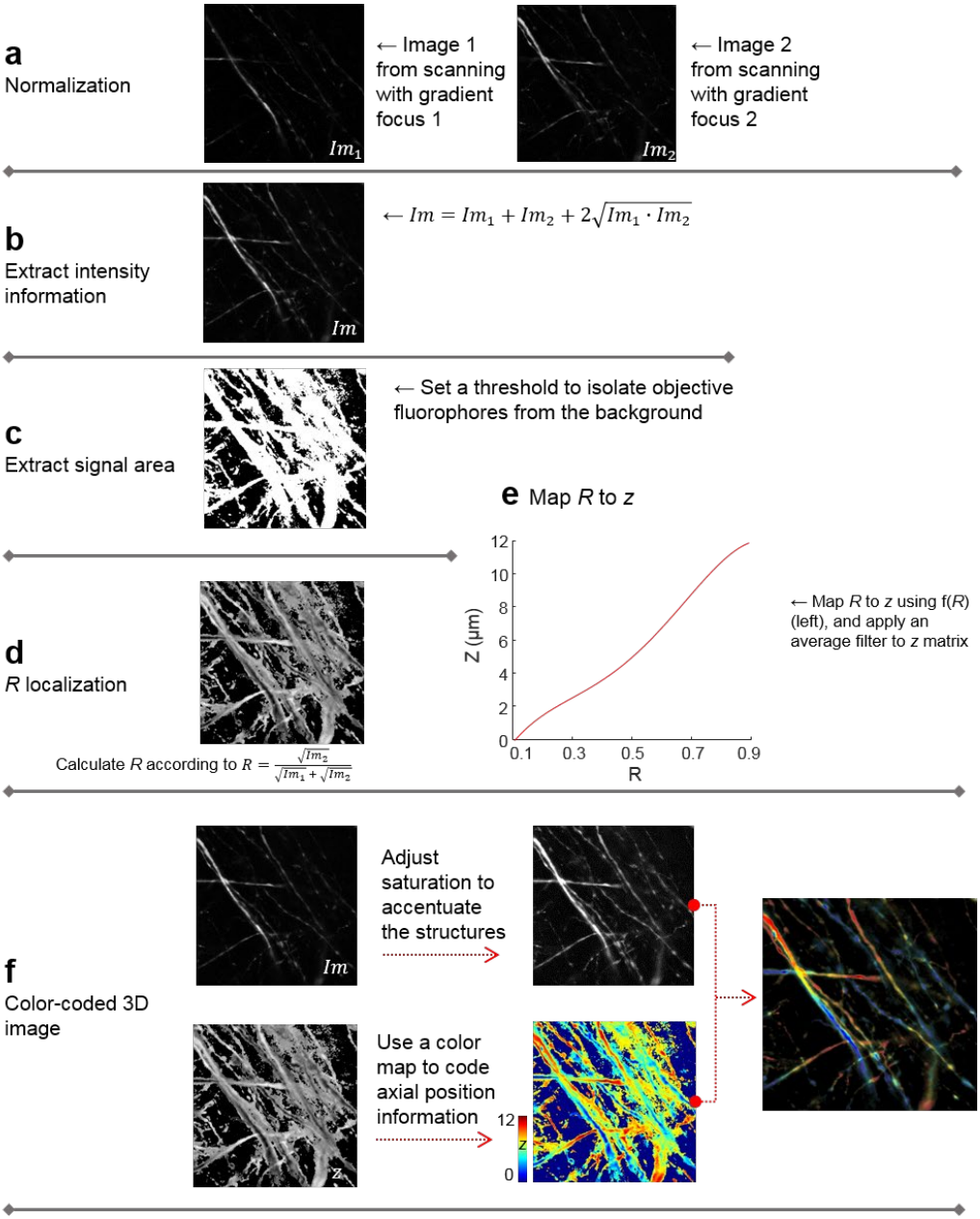

Fig. S10 Flowchart for axial location information extraction. Im_1 and Im_2 are paired images that generated by sequentially scanning with the gradient focus 1 and 2; R is the intensity ratio of Im_1 to Im_2. Function $f(R)$ is a ratio-depth mapping function, which maps R to z. Unit of z: μm.

Table S1. Data acquisition parameters.

Sample	Figures and Movies	Imaging mode	Single volume acquisition time (s)	Delay between successive acquisitions (s)	Volumetric imaging speed (Hz)	Volume size (μm^3)	Excitation power (mW)
Bead	Fig. 1c-f	Gauss-TPM	24	0	0.04	50×50×12	2
		Grad-TPM	4	0	0.25	50×50×12	6
Brain slice of CX_3CR1-GFP mouse	Fig. 2	Gauss-TPM	220	0	0.0045	200×200×22	12
		Grad-TPM	~37	0	0.027	200×200×22	~30
HEK293 cell (photobleaching)	Fig. 3a and Visualization 1	Gauss-TPM	13	2	0.07	100×100×13	~20
		Grad-TPM	2	13	0.07	100×100×12	45
RAW264 cell (macrophage)	Fig. 3b and Visualization 3	Grad-TPM	8	2	0.1	200×200×12	6
HepG2 cell (phototoxicity)	Fig. S3 and Visualization 2	Gauss-TPM	52	8	0.02	62.5×62.5×13	~20
		Grad-TPM	8	52	0.02	62.5×62.5×12	45

Table S2. Pupil phases of gradient focus pair

Ring	1	2	3	4	5	6	7	8	9	10
Outer diameter[a]	$\sqrt{1/40}$	$\sqrt{2/40}$	$\sqrt{3/40}$	$\sqrt{4/40}$	$\sqrt{5/40}$	$\sqrt{6/40}$	$\sqrt{7/40}$	$\sqrt{8/40}$	$\sqrt{9/40}$	$\sqrt{10/40}$
Phase of $GradF_1$[b]	2.90	1.07	-1.88	2.25	1.15	-1.20	-2.53	1.17	-2.67	-1.32
Phase of $GradF_2$[b]	3.07	1.00	-2.55	-1.49	1.84	-1.07	-2.11	-0.04	0.38	-1.22

Ring	11	12	13	14	15	16	17	18	19	20
Outer diameter	$\sqrt{11/40}$	$\sqrt{12/40}$	$\sqrt{13/40}$	$\sqrt{14/40}$	$\sqrt{15/40}$	$\sqrt{16/40}$	$\sqrt{17/40}$	$\sqrt{18/40}$	$\sqrt{19/40}$	$\sqrt{20/40}$
Phase of $GradF_1$	2.48	2.85	-2.23	-2.55	2.23	-2.67	-0.95	2.99	-1.81	-0.87
Phase of $GradF_2$	1.10	-0.23	1.10	2.48	0.97	2.01	2.45	2.38	2.85	2.94

Ring	21	22	23	24	25	26	27	28	29	30
Outer diameter	$\sqrt{21/40}$	$\sqrt{22/40}$	$\sqrt{23/40}$	$\sqrt{24/40}$	$\sqrt{25/40}$	$\sqrt{26/40}$	$\sqrt{27/40}$	$\sqrt{28/40}$	$\sqrt{29/40}$	$\sqrt{30/40}$
Phase of $GradF_1$	-1.98	-1.54	-1.24	-2.70	-1.86	-3.07	2.90	2.80	2.48	2.08
Phase of $GradF_2$	-3.14	-2.65	-1.49	-2.67	-1.61	-1.47	-2.65	-0.87	-2.67	-2.01

Ring	31	32	33	34	35	36	37	38	39	40
Outer diameter	$\sqrt{31/40}$	$\sqrt{32/40}$	$\sqrt{33/40}$	$\sqrt{34/40}$	$\sqrt{35/40}$	$\sqrt{36/40}$	$\sqrt{37/40}$	$\sqrt{38/40}$	$\sqrt{39/40}$	1
Phase of $GradF_1$	2.01	1.86	1.00	1.32	-0.75	0.90	-0.95	-1.52	0.97	-2.53
Phase of $GradF_2$	-3.09	-2.94	-2.38	2.85	-2.21	-2.55	0.87	-2.77	0.95	2.16

a: Normalized value.

b: $GradF_1$, gradient focus 1; $GradF_2$, gradient focus 2.